ELSEVIER

Nuclear Physics B (Proc. Suppl.) 85 (2000) 241–247

NUCLEAR PHYSICS B
PROCEEDINGS
SUPPLEMENTS

www.elsevier.nl/locate/npe

Virgo an Interferometer for Gravitational Wave Detection

R. Passaquieti * for Virgo collaboration. [a]

[a] *I.N.F.N.(Sez. di Firenze, Napoli, Perugia, Pisa, Roma1), L.N.F. Frascati, L.A.P.P. (Annecy), I.P.N.L. (Lyon), L.O.G. (Nice), E.S.P.C.I. (Paris), L.A.L. (Orsay).*

Gravitational waves propagating from rapidly accelerating star masses can be detected by means of interferometric techniques. The Virgo detector is a Michelson interferometer, with two $3\,km$ long Fabry-Perot cavities, that is going to be built in the countryside of Pisa (Italy). Principles of interferometric gravitational wave detection, and the main noise sources in the Virgo apparatus are treated. The Virgo optical scheme and its main components are also described. Finally, an overview on the status of works at the Virgo site is presented.

1. INTRODUCTION

The Einstein's theory of General Relativity foresees the existence of gravitational waves (GW) as a propagation way of the gravitational field. According to the same theory GW arise from the change of mass distribution, and propagate in vacuum at the speed of light.

The main difficulty in GW detection lies in the extreme weakness of their interaction with matter. Though more than 80 years have passed from their theoretical prediction GW have not yet been detected.

An indirect evidence of GW existence was given by the observations of Taylor and Hulse [1] of the binary pulsar system $PSR1913+16$. The measured orbital period decrement was consistent with GW energy loss within a fraction of 1%.

The early experiments on GW detection date back to the sixties, when J. Weber [2] built a series of resonant bars, at room temperature, sensitive to GW Fourier components around the main longitudinal resonant frequency ($\approx 1\,kHz$).

Beside resonant bars an alternative wide band GW detector is based on the use of a large laser interferometer with suspended optical components.

The Virgo project is a collaboration between the Italian I.N.F.N. and the French C.N.R.S. whose goal is to realize a $3\,km$ long laser interferometer for GW detection. The Virgo interferometer is designed to be sensitive in the frequency band from a few Hz up to a few kHz.

2. GRAVITATIONAL WAVES

In General Relativity the gravitational field is a perturbation of the *flat* space-time metric represented by the Minkowski's space-time metric tensor η_{ik}. Therefore the metric of a gravitational field is described by a more general symmetric tensor g_{ik} which contains all the information about the curvature of the space, and determines the infinitesimal space-time interval

$$ds^2 = g_{ik}dx^i dx^k \ . \qquad (1)$$

In the weak-field approximation, when the metric tensor can be written as

$$g_{ik} = \eta_{ik} + h_{ik} \ , \qquad (2)$$

the Einstein's gravitational field equation in vacuum can be linearized, and get the form of d'Alambert's *wave equation*

$$\frac{\partial^2 h_{ik}}{\partial x^j \partial x_j} = \Box h_{ik} = 0 \ . \qquad (3)$$

With an appropriate *transverse traceless* gauge choice (TT gauge) the most simple solution of equation (3), a monochromatic GW propagating along the $\hat{z}$ direction, can be described by the following tensor equation:

$$h_{ik}(t) = \left(h_+\hat{\varepsilon}^+_{ik} + h_\times\hat{\varepsilon}^\times_{ik}\right) exp\left[i\left(\omega t - k_z z\right)\right] \ , \quad (4)$$

where h_+ and $h_\times$ are the amplitudes of the two GW polarizations $\hat{\varepsilon}^+_{ik}$ and $\hat{\varepsilon}^\times_{ik}$ [3].

*INFN sez. Pisa, Via Livornese 1291 - 56010 - S. Piero a Grado (Pisa)- Italy. (E-mail: quieti@galileo.pi.infn.it)

3. INTERFEROMETRIC DETECTION

According to equation (4) in the case of a GW of amplitude $h(t)$, in a state of + polarization, propagating along the $\hat{z}$ direction, the space-time metric tensor of equation (2) becomes:

$$g_{ik} = \begin{pmatrix} -1 & 0 & 0 & 0 \\ 0 & 1+h(t) & 0 & 0 \\ 0 & 0 & 1-h(t) & 0 \\ 0 & 0 & 0 & 0 \end{pmatrix} e^{(ik_z z)} \; . \quad (5)$$

Let us consider this GW impinging the arms of a simple Michelson laser interferometer with free-falling optical components, and the two arms, of length L, oriented along the $\hat{x}$ and $\hat{y}$ directions.

Time elapsed by laser light in the round trip along each interferometer arm, between the beam-splitter and the end mirror, can be calculated integrating the light space-time interval $ds^2 = 0$ in the metric defined in (5). Round trip time for the light beam traveling along the $\hat{x}$ direction will be [4]:

$$\tau(x) \cong \frac{2L}{c} + \frac{h_0}{4\pi i f_G}\left[e^{4\pi i f_G L/c} - 1\right] \; . \quad (6)$$

Repeating the same calculation for the light travelling along the $\hat{y}$ direction we get a total light phase difference $\Delta\phi$, modulated by GW amplitude $h(t)$, which can be written as

$$\Delta\phi(t) \cong \frac{4\pi L}{\lambda_{ph}} \frac{\sin(2\pi f_G L/c)}{2\pi f_G L/c} h(t) \; , \quad (7)$$

where λ_{ph} is the laser light wavelength.

At the interferometer output the beams are made to interfere, and resulting power, collected by a photodetector, will be:

$$P_{out} = \frac{P_{in}}{2}\left[1 + \cos(\Delta\phi)\right] \; , \quad (8)$$

where P_{in} is the laser power at the interferometer input.

Finally interferometric GW detection resolves in a high sensitive phase modulation measurement.

To have an idea of the order of magnitudes involved in this kind of detection let us consider the case of GW produced in burst events. Supernova explosions and coalescing close binaries, occurring at distances up to the Virgo Cluster ($\approx 10\, Mpc$), have an expected amplitude [5] at Earth of the order of $h \approx 10^{-21}$. To detect such events it comes out, using equation (7), that an interferometer with arm length $L \approx 100\, Km$, requires a sensitivity of $\Delta\phi \approx 10^{-9}\, rad$.

4. NOISE SOURCES

Signal noise at the interferometer output, in absence of the real GW signal $h_{GW}(t)$, limits the sensitivity of the apparatus. If $S_n(f)$ is the power spectral density of the output noise, it is possible to define a fictitious GW signal whose amplitude spectral density is:

$$h_n(f) = \sqrt{S_n(f)}\ \left(1/\sqrt{Hz}\right) \; . \quad (9)$$

Detector efficiency is settled by the signal to noise ratio

$$SNR \equiv \sqrt{2\int_{-\infty}^{+\infty}\left[\frac{|h_{GW}(f)|^2}{S_n(f)}\right] df} \; . \quad (10)$$

The $SNR = 1$ value specifies the amplitude of the minimum detectable GW, defining the interferometer sensitivity.

4.1. SEISMIC NOISE AND THE VIRGO SUPERATTENUATOR

Noise source of greater intensity on a ground-based interferometer is due to soil vibrations produced by human activity and phenomena of geophysical and atmospherical nature.

Direct measurements of seismic noise on Virgo site are well described, in the 10 Hz frequency region, by the following empirical formula

$$x_{sn}(f) \cong \frac{\alpha}{f^2}\left(\frac{m}{\sqrt{Hz}}\right) \; , \quad (11)$$

where α is of the order of $\approx 10^{-8\div -6}(mHz^{3/2})$.

Virgo interferometer requires a sensitivity of the order of $h \approx 10^{-21}(1/\sqrt{Hz})$ at $10\, Hz$. It can be shown [6] that this level of sensitivity is reached bringing the mirror seismic noise down to a level of about $10^{-18}(m/\sqrt{Hz})$ with an attenuation of $200\, dB$.

Virgo achieves the anti-seismic filtering by means of an isolating suspension system, for its

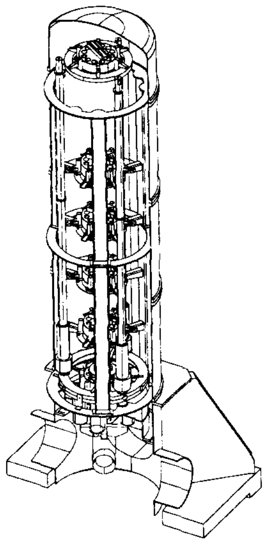

Figure 1. View of the Virgo superattenuator.

optical components, called *superattenuator*. Each superattenuator is essentially a multi-stage pendulum, with steel-made suspension wires, which works as a cascade of mechanical low-pass filters [7][8].

The superattenuator working principle is based on the multi-stage harmonic oscillator behavior.

The attenuation factor of the input horizontal vibrations, at the last stage of an N-stage pendulum, for frequency f much higher than pendulum resonances f_k, can be written as

$$A \propto \frac{C}{f^{2N}} , \tag{12}$$

where $C = \prod_{k=1}^{N} f_k^2$.

Each pendulum supports a variable number of metal spring blades according to the weight loaded along the chain position (from $\simeq 100\,kg$ up to $\simeq 1\,ton$). In this way the superattenuator becomes also a multi-stage vertical spring system. Each pendulum stage is able to attain an attenuation of about $40\,dB$, both in vertical and horizontal directions [9], in the frequency region above $10\,Hz$.

The whole pendulum chain is suspended to a pre-isolator stage called *inverted pendulum* [10]. This system consists of three long flexible metal legs of $\simeq 7\,m$ height, with a main horizontal resonance frequency less than $100\,mHz$, much lower than the $\simeq 0.5\,Hz$ minimum pendulum mode. An additional filter, at the top of the IP, sustains the chain and attenuates vertical noise transmission.

Thanks to this pre-isolator stage Virgo detection band, in the low frequency region, extends down to $\approx 4\,Hz$ [9], where pulsars and coalescing binaries are expected. In Virgo final design [11] there are 9 superattenuators with various numbers of stages, depending on the degree of locally requested seismic attenuation. A complete *long superattenuator* chain, whose sketch is reported in Fig. 1, consists of a five-stage pendulum $\simeq 10\,m$ high.

The last stage of the superattenuator sustain an intermediate mass called *marionette*. Mirrors are hung to the marionette by means of four steel wires. Together with the mirror the marionette sustain a massive cylinder called *reference mass*. The marionette and the reference mass allow the local control system to adjust the mirror alignment with the light beam, exerting forces on it, by means of magnetic coils.

A superattenuator prototype has been installed and tested in the Pisa Virgo group laboratory. Measurements have been carried out in atmospheric pressure and room temperature conditions, and final results have fulfilled Virgo requests[12]. In Fig. 2 is shown a graph of the prototype vertical transfer function (VTF), defined as the Fourier Transform modulus of the output to input ratio of vertical vibrations. An attenuation factor ranging between 10^{-9} and 10^{-13} in the frequency band $0-100\,Hz$ has been obtained. Easy coupling of the horizontal vibrations with the other degrees of freedom of the chain has complicated the measurements of the total horizontal transfer function (HTF). Nevertheless a stage by stage comparison between HTF and VTF have shown a better performance of the superattenuator in the horizontal direction. As a result the total HTF is expected to be orders of magnitude smaller than the total measured VTF.

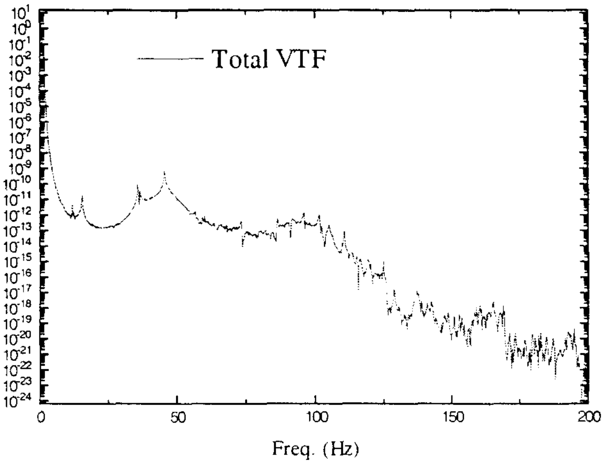

Figure 2. Graph of the total VTF of the superattenuator prototype.

4.2. NEWTONIAN NOISE

Gravitational gradient fluctuations, due to variations of mass distribution, cause unavoidable coupling of seismic noise with the interferometer optical components [13].

This effect is well described by a model that gives an estimate of the noise signal linear spectral density

$$h_N(f) \simeq 3 \cdot 10^{-17} \cdot \frac{1}{f^4} \left(\frac{1}{\sqrt{Hz}}\right) . \quad (13)$$

Newtonian noise is the limiting factor of seismic noise attenuation efficiency below a few Hz. In fact Newtonian noise, bypassing the suspension system, makes vain every further improvement in lowering the seismic noise below the Newtonian level.

4.3. THERMAL NOISE

The optical and mechanical components of Virgo do not operate in cryogenic conditions, so that when they are at equilibrium temperature $T(\simeq 20\,^0C)$ each degree of freedom gives rise to a random Brownian vibration of energy K_BT, where K_B is the Boltzmann constant. According to the *fluctuation-dissipation* theorem every system with mechanical impedance $Z(f)$, in thermal equilibrium, experiences a stochastic force whose power spectrum can be written as

$$F^2(f) = 4K_BTRe\,[Z(f)] . \quad (14)$$

The linear spectral density of thermal noise displacement depends on the dissipation mechanism. Virgo components operate in vacuum conditions, therefore the main dissipation mechanism is due to *internal friction*. In this case the noise spectrum has resonances in correspondence of the system mechanical modes f_k, behaves as $f^{-1/2}$ for $f << f_k$ and decreases as $f^{-5/2}$ for $f >> f_k$. Its amplitude decreases also increasing the mass and the mechanical quality factor Q.

Thermal noise is the limiting factor of the Virgo sensitivity in the frequency region from a few Hz up to a few hundreds Hz. For this reason a special attention is devoted in choosing materials with high Q values.

Silica coated mirrors, used in Virgo, have the first resonance mode at about $3\,kHz$ with a $Q \approx 10^6$.

4.4. SHOT-NOISE

Shot-noise is the limiting factor to Virgo sensitivity in the $10^2\,Hz$ frequency region. It is due to random fluctuations in the number of detected photons. These fluctuations give rise to uncertainty of output laser power, and consequently, as it comes out from equation (8), to a phase shift uncertainty [4] [9]

$$\Delta\phi_{shot} = \sqrt{\frac{4\pi\hbar c}{\eta\lambda_{ph}P_{in}}} \cdot \frac{\sqrt{1+\cos(\phi_0)}}{sin(\phi_0)} , \quad (15)$$

where ϕ_0 is the working point of the interferometer, and η is the photodetector efficiency. Equation (15) gets its minimum when the interferometer works in destructive configuration (*dark fringe*) with $\phi_0 = \pi$. In these conditions the shot-noise in terms of GW amplitude h is:

$$h_{shot} = \frac{1}{4\pi L} \cdot \sqrt{\frac{4\pi\hbar\lambda_{ph}c}{\eta P_{in}}} , \quad (16)$$

where L is the length of interferometer arms. The increase of input laser power reduces the level of shot-noise but increases the *radiation pressure* on mirrors. Radiation pressure is still linked to the particle-like nature of light, and has a signal noise spectral density [4] [6]

$$h_{rp}(f) = \frac{1}{mLf^2} \cdot \sqrt{\frac{\hbar P_{in}}{2\pi^3 \lambda_{ph} c}} , \quad (17)$$

where m is the mirror mass.

The contribution of shot-noise to total noise is dominant in the high frequency region, while radiation pressure noise dominates in the low frequency region. There exists an optimum power level that minimizes these contributions, but its level is so high that practically, as for Virgo, shot-noise is much higher than its optimum *quantum limit.*

4.5. LASER FREQUENCY AND POWER FLUCTUATIONS

Small asymmetries in arm length transform stochastic fluctuation Δf of laser frequency into phase fluctuations

$$\Delta\phi = \frac{2\pi}{c} \cdot \Delta L \cdot \Delta f . \quad (18)$$

In Virgo experiment the tolerance of optical path lengths is of the 1%, and laser frequency fluctuations are kept at a level lower than $10^{-6}(Hz/\sqrt{Hz})$. Also laser power fluctuation is a possible source of noise; to minimize its effects the interferometer is maintained in dark-fringe conditions by an active control system.

4.6. REFRACTIVE INDEX FLUCTUATIONS

Random fluctuations of molecular gas densities, along the optical path of laser beam, are at the base of refractive index fluctuations which result in phase shift fluctuations into the interferometer arms.

In order to reduce drastically this noise source the whole Virgo interferometer is contained into a very large vacuum vessel [11], within a volume of $\simeq 7000\, m^3$. The laser optical path is inside two vacuum tubes of $1.2\, m$ diameter and length $L = 3\, km$. According to Virgo requests residual gas pressure into the tubes and in correspondence of the optical elements must be of $\simeq 10^{-9}\, mbar$. In the upper chamber of the vacuum towers, where is located the superattenuator, residual gas pressure must be below $\simeq 10^{-6}\, mbar$.

5. VIRGO SENSITIVITY

The level of Virgo detection efficiency can be summarized by its design sensitivity curve of Fig. 3. This curve is a plot of the spectrum of a GW signal to which corresponds a value $SNR = 1$. The signal contributions of the main noise sources are plotted.

The graph shows that Virgo detection band will extend from $4\, Hz$ up to a few kHz. It is clear how the superattenuator reduces the seismic noise to negligible values. The $4\, Hz$ minimum value of detectable frequency is in correspondence of the crossing point of seismic and Newtonian noise curves.

In the high frequency region Virgo sensitivity is of $\approx 3 \cdot 10^{-23}(1/\sqrt{Hz})$.

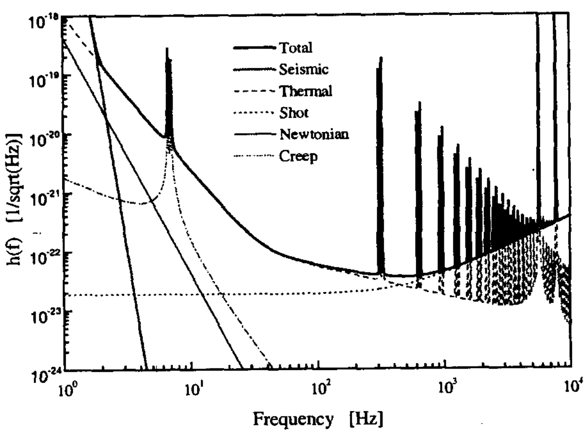

Figure 3. Virgo sensitivity.

6. VIRGO OPTICAL SCHEME

6.1. FABRY-PEROT CAVITIES

From equation (7) it is quite evident that the low frequency sensitivity amplitude, and the high frequency limit of detection band are proportional to the interferometer arm length L. For example a $1\,kHz$ Michelson interferometer requires an arm length $L \simeq 75\,km$.

For practical reasons, in the interferometers on the way to be built, the optical path length is made larger by folding into arms of fixed length. In Virgo the optical path folding is obtained enhancing the simple Michelson interferometer optical scheme by means of two *Fabry-Perot resonant cavities* of length $L = 3\,km$ [11] [14]. The cavities are obtained, as shown in Fig. 4, inserting in each arm after the beam-splitter a semi-reflecting plane mirror.

In a Fabry-Perot laser interferometer the output phase shift due to a monochromatic GW signal becomes:

$$\Delta\phi(t) = \frac{8LF}{\lambda_{ph} \cdot \sqrt{1 + \left(\frac{4F f_G L}{c}\right)^2}} \cdot h(t) \;, \qquad (19)$$

where F is the *cavity finesse*. In this case the average optical path length is:

$$L_{FP} \simeq 4FL/\pi \;. \qquad (20)$$

The finesse of Virgo cavities is $F = 50$; than along each arm the effective optical path length is $\approx 100\,km$. Semi-reflecting cavity mirrors need to have very low-value absorption coefficient in order to avoid laser beam degradation. Far end-mirrors have a concave surface to avoid beam defocusing.

6.2. POWER RECYCLING

Presently the power level of lasers does not allow to lower the shot-noise to its quantum limit, but it is still possible to amplify this power by *recycling* techniques. When working in dark-fringe conditions almost all the laser power stored into the interferometer arms is back-reflected to the input laser and lost. This power can be re-injected into the interferometer placing a *recycling mirror* between the beam-splitter and the laser source, so to realize a resonating cavity for the back-reflected beam. The recycling mirror views the rest of the interferometer, after the beam splitter, as the second reflecting mirror of the *recycling cavity*. Light into the recycling cavity is in phase with the laser source, and the control system maintains this resonating condition.

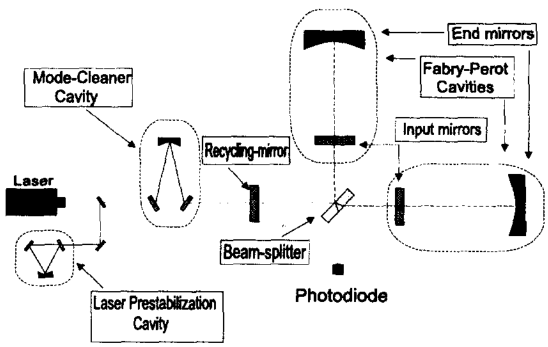

Figure 4. Optical scheme of the Virgo interferometer.

In Virgo [11] the laser source is of Nd: YAG type, with a power of $20W$ and a wavelength $\lambda_{ph} = 1064\,nm$. After recycling the input laser beam has a power of about $500\,W$.

6.3. LASER STABILIZATION AND MODE-CLEANING

Frequency stabilization of Virgo laser is obtained by means of a pre-stabilization cavity, maintained in resonance with the laser beam by the control system, which ensure a stability of $10^{-4}(Hz/\sqrt{Hz})$. The required frequency stability of $10^{-6}(Hz/\sqrt{Hz})$ is reached by the control system, taking as a reference one of the two Fabry-Perot cavities.

Once the laser frequency has been stabilized the beam is filtered by its spurious modes in a triangular cavity, called *mode-cleaner*.

7. VIRGO APPARATUS AND FACILITIES

In Fig. 5 is shown the scheme of the Virgo apparatus that is going to be installed in Cascina, in the countryside of Pisa. The *central building*, that covers an area of about $1000\,m^2$, includes the group of towers at the interferometer crossing point. Each tower contains one superattenuator chain suspending a proper optical device: the *laser injection* and *detection benches*, the *beam-splitter mirror*, the *recycling mirror* and the *in-*

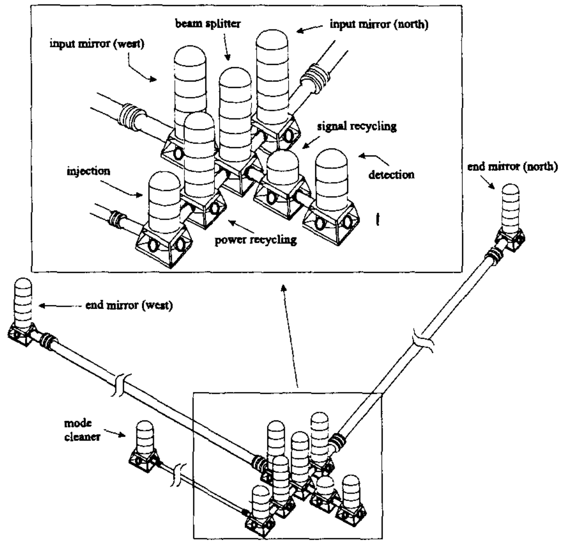

Figure 5. Scheme of the Virgo apparatus.

put mirrors of the 3 km Fabry-Perot cavities. The central building includes also some technical laboratories and cleaning rooms for installation and maintenance of the components of the apparatus.

The two 3 km long tubes depart from the North and West sides of the central building, and run through two concrete metal-structure tunnels. At the far end of the tunnel two smaller buildings contain the *end mirror* towers.

Finally on the West side a 144 m long tunnel contains the tube that connects the laser input tower to the mode-cleaner tower placed into a separate small building.

The Virgo facility consists also of other buildings that contain technical equipment for environmental maintenance and computing systems.

Presently the central building, the mode-cleaner building and its tunnel, with the tube inside, are ready, and the foundations works for the two 3 km tunnels have begun. Installation is in deep progress. Mode cleaner, injection and detection superattenuators are installed, and successfully tested; vacuum tests on mode-cleaner tube and mode-cleaner tower are in progress.

8. CONCLUSIONS

According to the time-schedule the first goal will be the installation of an unfolded Michelson interferometer in the central area. Many activities will be performed on this interferometer to test the performance of all optical and mechanical components, in their working conditions. Moreover the experience made will help in a deeper characterization of all possible noise sources to improve the final detector sensitivity.

REFERENCES

1. J. H. Taylor, Rev. Mod. Phys. **66** (3) (1994) 711.
2. J. Weber, Phys. Rev. **117** (1960) 306.
3. C. W. Misner K. S. Thorne and J.A. Wheeler, Gravitation, W. H. Freeman and company, New York,(1973), ch.35.
4. P.R. Saulson, Interferometric Gravitational Wave Detectors, World Scientific, Singapore, (1994).
5. K.S. Thorne in Three hundred years of gravitation, S. W. Hawking and W. Israel editors, Cambridge University Press, (1987), Ch 9.
6. A. Giazotto, Physics Reports **182** (1989) 365.
7. S. Braccini et al., Rev. Sci. Instrum. **67** (8) (1996) 2899.
8. M. Beccaria et al., Nucl. Instr. and Meth. in Phys. Res. **A394** (1997) 397.
9. B. Caron et al., State of the Art of the Virgo Experiment, in Proc. of the International Conference on Gravitational Waves: Sources and Detectors (March 1996), Pisa, Italy.
10. G. Losurdo et al., Rev. Sci. Instrum., Vol. 70, No. 5, (May 1999), 2507.
11. The Virgo collaboration, Final Design Report, (1997), Pisa, Italy.
12. F. Frasconi et al.,Performances of the Superattenuator Chain of the Virgo Experiment, Proc. of XXXIVth Recontres de Moriond on Gravitational Waves and Experimental Gravity, January 1999.
13. M. Beccaria et al., Class. Quantum Grav. **15** (1998) 3339.
14. M. Bernardini et al., Nuclear Physics (Proc. Suppl.) **54B** (1997) 179.